Heliyon 11 (2025) e42807

Contents lists available at ScienceDirect

Heliyon

journal homepage: www.cell.com/heliyon

Research article

Effect of photoinduction in PANi/TiO_2 heterogeneous structure on conductance of PANi component

Huyen Ngoc Duong [a,*], Tan Van Le [b]

[a] Faculty of Electrical Engineering Technology, Industrial University of Ho Chi Minh City, 12, Nguyen Van Bao, Go Vap District, Ho chi Minh City, Viet Nam
[b] Faculty of Chemistry, Industrial University of Ho Chi Minh City, 12, Nguyen Van Bao, Go Vap District, Ho Chi Minh City, Viet Nam

ARTICLE INFO

Keywords:
TiO_2
PANi
PANi/TiO_2 heterostructure
Photoelectrochemical
Photocatalysis

ABSTRACT

A heterostructure consisting of a PANi and a TiO_2 layer was chemically deposited consecutively on a glass substrate to investigate the effect of photoinduction in the structure on the conductance of the PANi component. It has been found that in response to the excitation light, the conductance of the PANi component in the PANi/TiO_2 heterostructure exhibits a distinct mode to be different from that of a single pristine PANi layer. The features account for the effects of photoelectronic and electrochemical processes that associate with the photoinduction in the PANi/TiO_2 heterostructure. The photoelectronic effect involves the appearance of the excess charges photogenerated inside the heterostructure on the depletion region. Due to the thermal diffusion of excess charges across the heterojunction, the width of the depletion is altered, leading to a modification in the conductance of the structure components, including the PANi. The electrochemical effect, on the other hand, relates to the appearance of the reactive oxygen species of $O_2^{\bullet-}$, $OH^{\bullet-}$ and H^+ that are created outside the heterostructure surface due to the photoinduction. Acting as strong oxidants, the species play the role of extra acceptor-like dopants and donor dedoping agents that modify the oxidation state and then the hole density of the p-type semiconductor PANi. The initial modification causes a sudden drop in PANi conductance at the start. As the exposure is further prolonged, the oxidation degree of the PANi component is further altered; the initial PANi emeraldine salt is gradually inverted to the emeraldine base, resulting in a conversion of its conductance. The combination of two modifications is explained for the mixing responses in the conductance of the PANi component and the U-turn shape of its baseline.

1. Introduction

It is well known that photocatalysis involves the photoinduced effect occurring in nanostructured semiconductors upon exposure to sunlight [1,2]. The photoinduction process gives rise to highly reactive oxygen species that exhibit the ability to sterilise microbial cells, bacteria, or decompose, degrade, or mineralize a variety of pollutants, such as organic molecules, toxic and harmful gases, and heavy metal ions (see Fig. 1a). With the growing environmental problems, semiconductor photocatalysis is emerging as one of the most efficient and sustainable means to solve the issues [3–8]. Out of the potential semiconductor photocatalysts, titanium dioxide (TiO_2), a typical wide bandgap semiconductor of *n*-type, has been the most exploited due to its high efficiency, low cost, stability, safety and

* Corresponding author.
E-mail address: duongngochuyen@iuh.edu.vn (H.N. Duong).

https://doi.org/10.1016/j.heliyon.2025.e42807
Received 16 July 2024; Received in revised form 16 February 2025; Accepted 18 February 2025
Available online 19 February 2025
2405-8440/© 2025 Published by Elsevier Ltd. This is an open access article under the CC BY-NC-ND license (http://creativecommons.org/licenses/by-nc-nd/4.0/).

availability. However, the TiO_2 photocatalyst confronts restrictions owing to the narrow photocatalytic region in UV light ($\lambda < 400$ nm), high charge recombination rate, low absorption surface, etc., that can hinder its practical application [9].

Many efforts have been proposed to improve the photocatalytic performance of the TiO_2, including doping, surface modification, bandgap modification, inorganic or organic adsorbate coating, etc., [10–12]. Among the proposals, the heterogeneous structure created by coupling the TiO_2 with a suitable bandgap semiconductor has shown to be the most effective approach [13–17]. In the heterostructure, the visible light cannot be absorbed by the TiO_2 but by the narrower bandgap counterpart, resulting in pairs of electron-hole. Due to the coupling, the photogenerated electrons and holes can transfer from the narrow bandgap semiconductor to the TiO_2 and then participate in the photocatalytic process. Concerning the cost and processing, non-metal modification of TiO_2 photocatalyst is the most attractive; for that reason, the semiconducting polymer arises as an effective component in realising efficient TiO_2 heterogeneous photocatalysts [18–20].

Among the semiconducting polymer group, polyaniline (PANi) is one of the most explored materials due to its easy synthesis, low cost, high stability, high degree of processability, tunable conducting and optical properties, etc. [21,22]. Depending on the oxidation and protonation level, the PANi behaves as a *p*-type semiconductor with bandgap spreading in a wide range, namely 3–4 eV for leucoemeraldine and emeradine base, 1.5–2.2 eV for pernigraniline, and 2.7 eV for emeraldine salt [23–25]. These aspects facilitate many specific applications, such as electronics, sensors, actuators, photovoltaic cells, photocatalysts, etc., [26–29].

Regarding photocatalysis, the PANi/TiO_2 heterostructure has been shown to be efficient in both UV and Vis due to the synergistic effect of both components [20,30–33]. The improvement accounts for the effective visible light sensitisation of TiO_2 by the PANi and the PANi/TiO_2 heterojunction that is considered to be a critical factor in reducing the charge recombination and increasing the photocatalytic efficiency. However, most works made on PANi/TiO_2 heterostructures have focused mainly on the synthesis methods and photocatalytic features; the photocatalysis process in the structure needs to be further investigated via experiments to verify existing concepts or to suggest other variants. From the physicochemical viewpoint, the photoinduction process in the PANi/TiO_2 heterogeneous structure, as exemplarily shown in Fig. 1b, can split into two stages: (1) photoelectronic involves the electron-hole pairs photogeneration, segregation, and migration to the component surfaces, this process usually accompanies the charge recombination and charge transfer between PANi and TiO_2 components; (2) electrochemical relates to the redox reactions between the reductive electrons, oxidative holes, and the O_2, H_2O molecules adhered to the heterostructure surfaces, forming reactive oxygen species of $O_2^{\bullet -}$, $OH^{\bullet -}$ and H^+ as well as numbers of secondary reactive radicals in following sequence redox reactions. The formation of those reactive oxygen species relies on the content of O_2, H_2O in the medium and, for environmental remediation, plays a critical role in degrading or mineralising a variety of pollutant molecules in the surrounding medium. The charge photogenerated and transferred processes in the first stage alter the charge density and the electronic configuration of the heterostructure constituents, namely the PANi and TiO_2 components [34]. The reactive radicals, on the other hand, have revealed the electrochemical oxygen reduction reaction to the semiconducting polymer PEDOT as a means of outer-sphere electron transfer and the addition of molecular oxygen reduction products to oxidised and reduced forms [35,36]. In the same manner, the reactive radicals generated outside the PANi/TiO_2 heterostructure in turn are expected to affect the oxidation state of the PANi component. Due to the susceptibility of PANi to physical and chemical interaction, the effects of the photoinduction process in the PANi/TiO_2 heterostructure then will be reflected in the PANi conductance. Based on that assumption, a double structure consisting of a PANi layer and a TiO_2 layer was made on the glass substrate to verify the response of PANi layer conductance as the structure was exposed to the excitation lights. The air, where the experiment was carried out, was considered to be an inert medium for the conductance measurement but to consist of O_2 and H_2O for the photoinduction taking place. The excitation lights were monochromatic LEDs whose wavelengths were in the range of UV, blue, and red regions. Upon exposure to the excitation light, the modification of PANi conductance was used to analyse and deduce the effects of the photoinduction in the PANi/TiO_2 heterostructure.

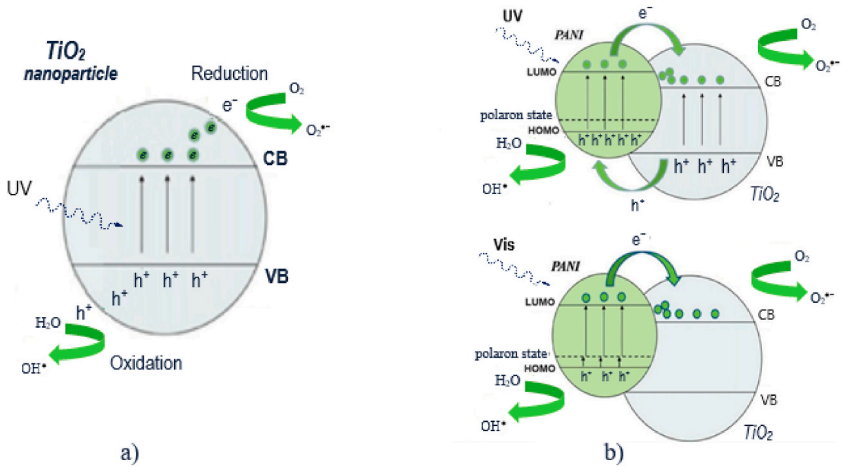

Fig. 1. a) Mechanism of the redox photogenerated charges in a TiO_2 semiconductor nanoparticle. b) Mechanism of the generation of reactive oxygen radicals under UV and visible light by a PANi/TiO_2 heterogeneous photocatalyst.

2. Materials and methods

Chemical synthesis methods were used to make the PANi/TiO_2 heterostructure by growing a PANi and depositing a TiO_2 thin layer separately on a glass substrate as shown in Fig. 2a. The PANi thin layer was grown by *in-situ* oxidative polymerisation following the common routine [37,38], where the starting precursor was aniline (99.5 %, Merck & Co., Inc.) and the oxidant was ammonium persulfate (APS, Kanto Chemical Co. Inc.), respectively.

The next TiO_2 thin layer was made in sequence on the PANi layer by thermal hydrolysis of titanium trichloride ($TiCl_3$, Sigma-Aldrich) using a similar procedure [39]. The PANi-coated glass plate was immersed into a solution of 40 mM $TiCl_3$ and then was heated up to a temperature of 80 °C to ignite the hydrolysis of the titanium precursor. During the decomposition of $TiCl_3$, a thin layer of TiO_2 was deposited over the PANi surface, forming a PANi/TiO_2 heterostructure on the glass substrate. After 2 h, the glass was pulled out, washed, and rinsed in 1.0 M HCl solution, and dried in a desiccator.

The structure, surface morphology, and cross-section of the PANi thin layer and the PANi/TiO_2 heterostructure were characterised using XRD (Panalytical) and FESEM (Hitachi-S4800) while the chemical and electronic structures were analysed by Raman spectroscopy (Carry) and UV–Vis absorbance spectroscopy (Visco V 750).

The experiment scheme set up to verify the light response of the PANi layer in the PANi/TiO_2 heterostructure was shown in Fig. 2b. The PANi layer resistance was measured by a Keithley 2000 connected to a computer, and then the light sensitivity was calculated as the ratio of $\Delta R/R_0$, where R_0 is the initial resistance of the layer and $\Delta R = R - R_0$. The test was carried out in the air at room temperature. All the light sources and sample were confined in a closed chamber to reduce the influence of surrounding environment on the test results.

To determine the wavelength dependence, excitation lights with wavelengths around 369.0 nm, 396.0 nm, 447.0 nm and 663.0 nm respectively, from monochromatic LEDs whose spectra are shown in Fig. 3, were used. After each testing, the sample was reactivated in 1.0 M HCl solution to fully recover its conductance and put in the test chamber for the next measurements. The distance between the LED sources and PANi/TiO_2 was adjusted to get the light intensity around 2.0 W/m^{-2} to reduce thermal effect on layer conductance. The excitation light was modulated in a rectangular pulse form by setting the light on in 600 s and off in 720 s consecutively.

3. Results and discussion

3.1. Result

The surface morphology and cross-section of PANi and PANi/TiO_2 structures are shown by SEM images in Fig. 4. The pictures in Fig. 4a and c indicate that the PANi layer is uniformly coated on the glass substrate with a smooth surface and a thickness around 90 nm. The even continuity in the PANi/glass interface indicates a strong bond between PANi and the hydrophobic surface of glass [36,37] as confirmed by the nanomechanical characterisation [40]. The images in Fig. 4b and d reveal the TiO_2 agglomerations consisting of long grains with a mean diameter around 30–40 nm and an aspect ratio around 0.3–0.5 randomly distributed over the PANi surface. The appearance of air gaps, craters, and cavities at the PANi/TiO_2 boundary implies that the binding between the TiO_2 grains and the PANi is rather weak (Fig. 4d). The interaction between the *p*-type semiconductor of PANi and the *n*-type semiconductor of titanium radicals during the nucleation and growth may affect the morphology of TiO_2 grains deposited on the PANi surface.

The XRD pattern made of the TiO_2 deposited on the PANi layer (Fig. 5) consists of diffraction peaks standing for the rutile structure; namely, the main peak observed at 2θ of 27.63° is assigned to (110) plane refraction, while the other peaks, observed at 2θ of 36.18°, 41.34°, 54.42°, 56.38°, 62.72°, and 68.88°, stand for the refraction at (101), (111), (211), (220), (002), and (301) planes, respectively (JCP2.2CA number 00-021-1276) [34,39]. The predominance of the ruttile structure in the resulting TiO_2 is accounted for by the effect of the strong HCl acidic aqueous medium during the hydrolysis of Ti precursor [39].

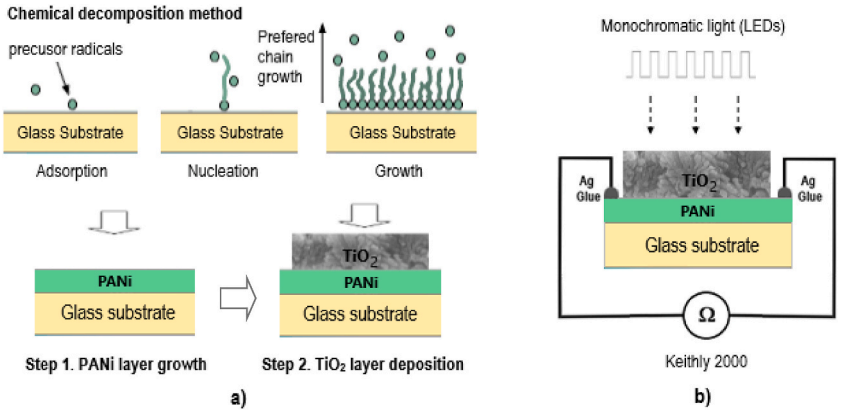

Fig. 2. a) Scheme of growing PANi and depositing TiO_2 thin layer separately on glass substrate. b) Experiment set up to measure the resistance of the PANi layer in the PANi/TiO_2 heterostructure in response to excitation light.

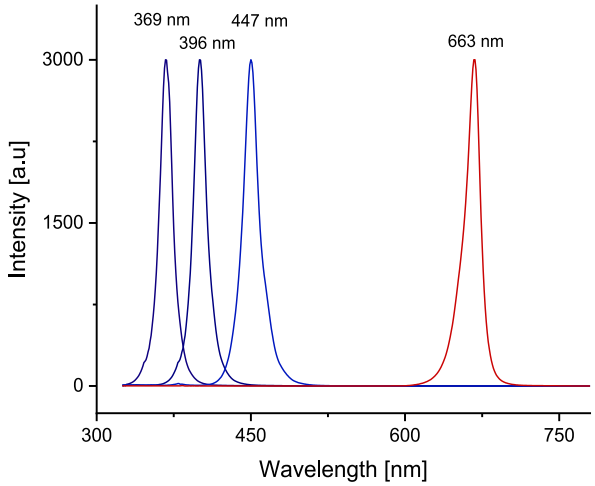

Fig. 3. Spectra of monochromatic LEDs used as photoexcitation sources in the experiment.

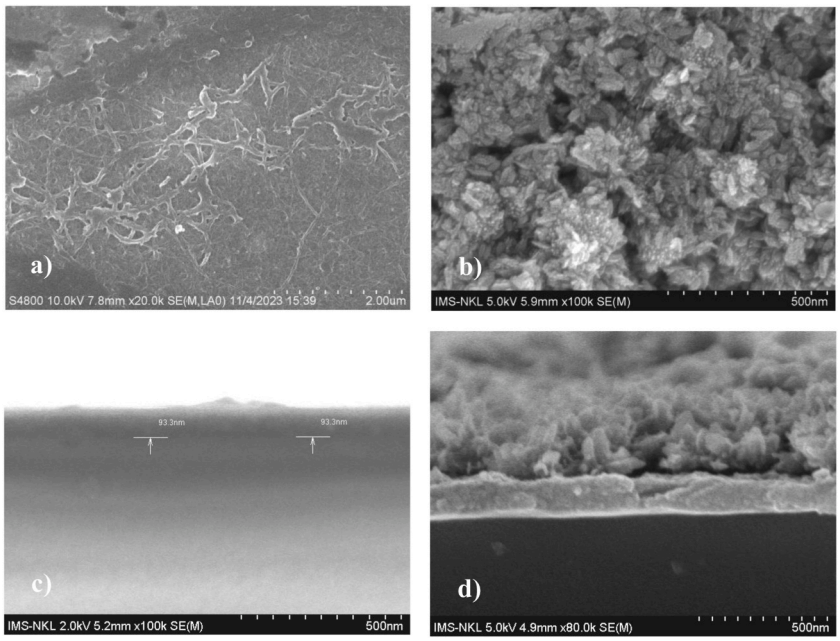

Fig. 4. a) FESEM images of PANi surface; b) PANi/TiO_2 structure surface; c) PANi cross-section; and d) PANi/TiO_2 structure cross-section.

Raman spectra of the TiO_2, PANi, and PANi/TiO_2 structure on glass are shown in Fig. 6. The Raman spectrum of TiO_2 segregated on the reactive medium (Fig. 6a**)** reveals two main Raman shifts peaking at 610 cm^{-1} and 441 cm^{-1} standing for A_{1g} and E_g vibration modes of rutile (R) while a small peak at 151 cm^{-1} is assumed to be a combination of the B_{ig} vibration mode from rutile and the E_g mode from a small trace of anatase (A) [41]. Coupling with PANi, the A_{1g} and E_g vibration modes of rutile (R) shift to 606 and 439 cm^{-1}, respectively, while the 151 cm^{-1} band standing for B_{ig} (R) and E_g (A) mode reduces and shifts to 137 cm^{-1} (see Fig. 6b and d**)**. The reduction and shift of vibration modes of TiO_2 indicate the effect of PANi on the electronic structure of TiO_2. On the other hand, the Raman spectrum of PANi/TiO_2 in Fig. 6d also exhibits the modification in vibration modes standing for PANi because of coupling with TiO_2. Referring to the Raman assignment for PANi [42–45], the broad band around 1180 cm^{-1} is assumed to be the combination of C–H in-plane bending vibrations of the benzenoid and semiquinonoid rings peaking at 1181 cm^{-1} and at 1157 cm^{-1}, respectively [44]. The peak at 1249 cm^{-1} is associated with the benzenoid ring deformations vibration, while the peak at 1329–1338 cm^{-1} is assigned to the C–N^+ stretching of charge delocalisation related to polaronic structures [45]. The peak at about 1506 cm^{-1} is assigned to the N–H deformation vibrations associated with the semiquinonoid structures. For quinonoid rings, the C=N stretching vibration likely stands at around 1480 cm^{-1} while the C=C stretching is assigned to 1598–1620 cm^{-1} range. For the Raman shift in a range below 1000 cm^{-1}, the peak at 811 cm^{-1} is assigned to the benzene-ring deformations, and the peak observed at 578 cm^{-1} can be connected to the amine

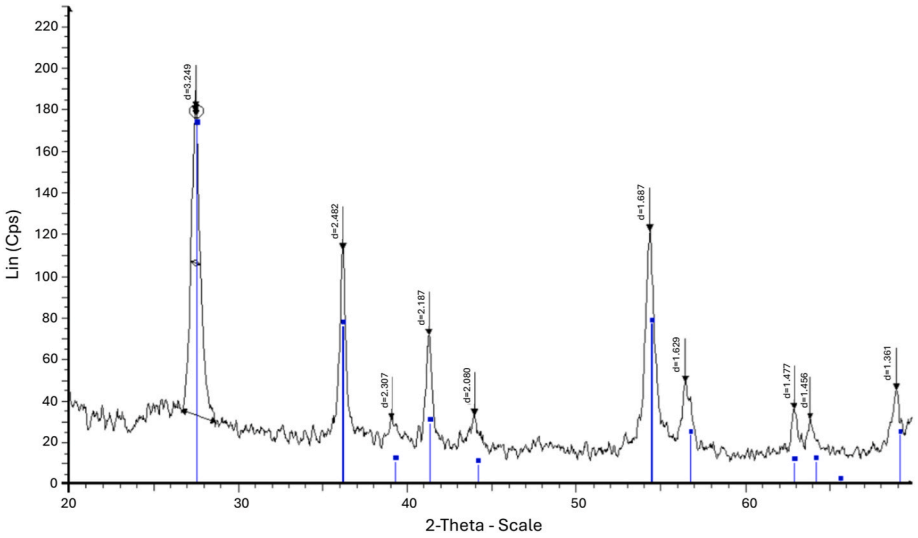

Fig. 5. XRD spectrum of TiO_2 deposited on the PANi surface in the PANi/TiO_2 heterostructure.

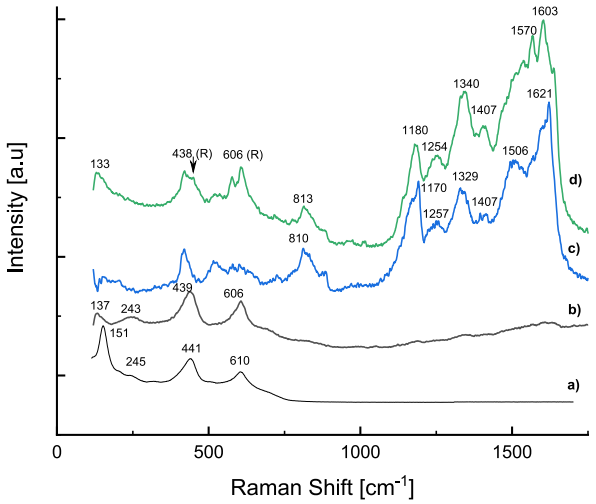

Fig. 6. Raman spectra of PANi and PANi/TiO_2 structure: a) TiO_2 deposited in the hydrolysis medium; b) TiO_2 particle on PANi surface; c) PANi layer on glass; d) PANi/TiO_2 structure.

deformation vibrations of the emeraldine salt [42. 45]. Out-of-plane deformations of the rings relate to the peaks at 522 and 418 cm^{-1}. The most striking point observed in the PANi/TiO_2 spectrum is the shift in the position and the increase in the intensity of the 1180, 1249 and 1338 cm^{-1} vibration modes that are accounted for an increase in the semiquinonoid, benzene ring deformation, and C–N^+ structure. Since the semiquinonoid structure is considered as a criterion of the oxidation state, the C–N^+ structure involves the polaron lattice, and the benzene ring deformation increases the charge mobility in PANi chain [43,44], the Raman spectra indirectly indicate the role of TiO_2 in enhancement of the emeraldine salt in the PANi/TiO_2 structure.

The absorptance UV–Vis spectra of the TiO_2 deposited in the reactive solution, the PANi layer growth on the glass substrate, and the PANi/TiO_2 structure are shown in Fig. 7a, and as a reference the spectra of monochromatic LEDs used as excitation sources are enclosed. The TiO_2 reveals a spectrum with the absorption edge around 430 nm (2.88 eV). On the other hand, the spectrum of PANi/TiO_2 consists of two bands centred at 438 nm (~2.83 eV) and 335 nm (3.70 eV) and a very broad band extending over the infrared region. These bands are assigned to the polaron → π*, π → π* and π → polaron transitions, standing for the absorption bands of emeraldine salt that is exemplarily shown in Fig. 7b [23–25,46]. The PANi layer, however, shows a spectrum composed of adsorption bands centred around 563 nm (~2.20 eV), 395 nm (~3.14 eV) and 318 nm (~3.90 eV). The absorption band at 563 nm is assigned to the transition π → π* from emeraldine base, the left bands at 395 nm and 318 nm are assumed to be a combination of absorption bands originated from the transitions π → π* of the benzenoid ring of both emeraldine base and emeraldine salt and polaron → π* from emeraldine salt (Fig. 7b). The UV spectra also reconfirm the effect of TiO_2 in the enhancement of the emeraldine salt and then the PANi

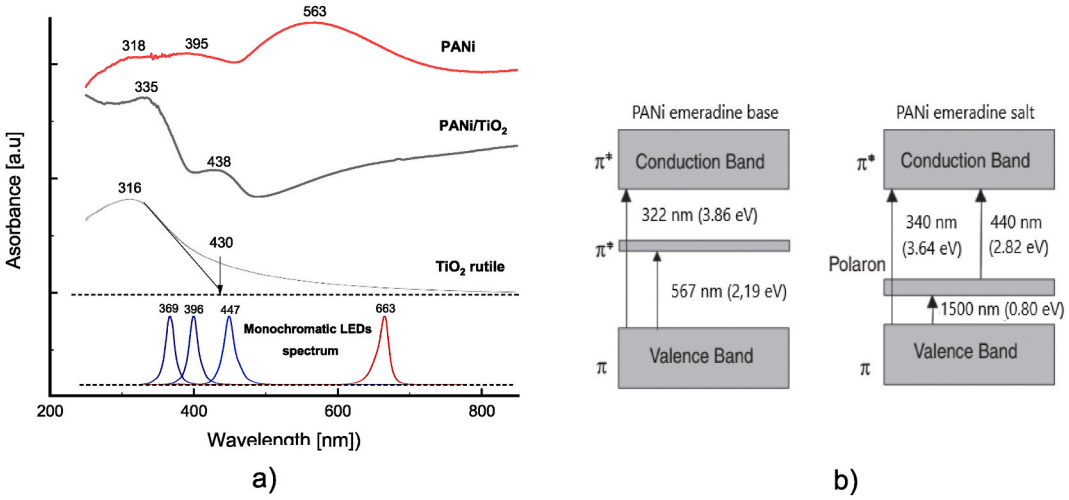

Fig. 7. a) UV–Vis spectra of PANi and PANi/TiO_2 heterogeneous structure. b) Absorption band of emeraldine base (PANI-EB) and emeraldine salt (PANI-ES).

component conductance in the PANi/TiO_2 heterogeneous structure [29,47].

With respect to the light response, both the pristine PANi and the PANi component layer in the PANi/TiO_2 heterostructure are sensitive to the excitation light but in distinctive modes. The resistance of the pristine PANi layer decreases when the excitation light is on and recovers when the light is off, i.e., the light sensitivity $\Delta R/R_0$ is negative (Fig. 8a). The light sensitivity for all excitation lights is almost independent of the excitation light wavelength (~excitation photon energy). Over the irradiated time, the resistance baseline (dotted) tends to descend with long wavelength and rises with short wavelength excitation light. On the contrary, the resistance of the PANi component layer in the PANi/TiO_2 heterostructure shows a mixing response to excitation light over irradiated time. At the starting irradiation, the light response of the PANi component layer also shows a negative mode and depends on the excitation light wavelength; the shorter the light wavelength, the higher the light sensitivity in accompaniment with a rapid reduction of the resistance baseline as shown in Fig. 8b. However, in the following, the light sensitivity of the PANi component fast declines in magnitude and converts from negative to positive mode at the point marked by CP (Conversion Point). Accordingly, the baseline also shows a fast reversion and makes a U-turn. On the other hand, the light response of the PANi component layer to the excitation light of wavelength 663 nm reveals a mode similar to that of the pristine PANi layer, namely showing an identical negative sensitivity over irradiation time and no U-turn in the resistance baseline.

3.2. Discussion

From the physics point of view, the conductance of the PANi layer relies on the density of delocalised electrons arising from the π bond structure (PANi chain) that in turn, is susceptible to the physical and chemical interactions. During the synthesis, the Cl^- ions and persulfate radicals acting as acceptor-like dopants incorporated into the π bond structure give rise to polaron or bipolaron bands within the PANi bandgap and convert the materials to be *p*-type semiconductors. Due to the susceptibility of the π structure, the electronic state of the PANi can be further modified by physical and chemical interactions as exposed to the adjacent environment. As an example, the physical adsorption of oxidative or reductive gases available in open air has been shown to affect the PANi conductance and enabled the development of a variety of gas sensors. In the same manner, upon exposure to the excitation light, the decrease in resistance (or increase in conductance) of the pristine PANi layer, as in Fig. 8a, then can be explained simply by an addition of electrons and holes resulting from photoexcitation, a physical interaction. The overlap between the absorption band of the pristine PANi layer (Fig. 7) and the spectra of excitation lights (Fig. 3) can account for the light response of the pristine PANi layer.

In the PANi/TiO_2 heterostructure, the PANi component layer shows a mixed light response that can be explained as a combination of both effects of the photoelectronic and the electrochemical processes that occur inside and outside of the PANi/TiO_2 heterojunction. From the viewpoint of physics, under normal conditions, the band structures of the *p*-type semiconductor PANi, *n*-type semiconductor TiO_2 and the *p-n* PANi/TiO_2 heterogeneous structure are shown as in Fig. 9a and b. In the *p-n* PANi/TiO_2 heterostructure, the difference in charge densities from both sites leads to a thermal charge diffusion over the interface, setting up a depletion region there. Upon exposure to the excitation light, the appearance of the excess electrons and holes photogenerated in both PANi and TiO_2 sites will alter the depletion width, and then modify the conductance of the PANi component layer (Fig. 9c) [34]. Regarding the electrochemical effect, the excess oxidative electrons accumulated on TiO_2 surface react with the O_2 in the open air, creating $O_2^{\bullet -}$ while the excess reductive hole accumulated on the PANi surface reacts with adjacent H_2O molecules from moisture, forming hydroxyl radical $OH^{\bullet -}$ and hydrogen radical H^+. From the viewpoint of electrochemistry, the reactive oxygen species can perform an electrochemical oxygen reduction reaction on the semiconductor PANi in a similar way to the semiconducting polymer PEDOT [35,36]. A scheme of the oxidation and reduction generally taking place in PANI emeraldine is shown in Fig. 10 as a reference. Acting as strong oxidants, the

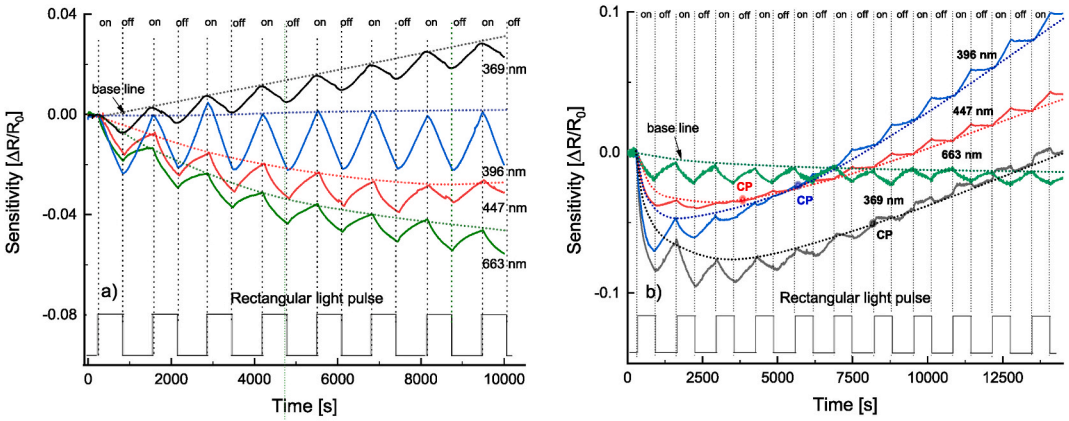

Fig. 8. a) Light sensitivity of uncoupling PANi and b) light sensitivity of the coupling PANi in the PANi/TiO_2 heterostructure.

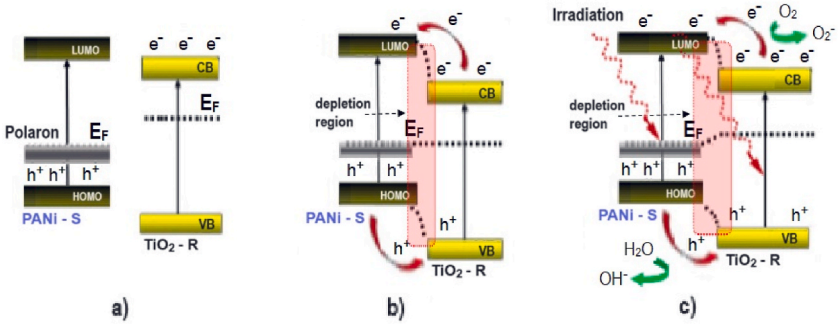

Fig. 9. Mechanism of charge exchange in the PANi/TiO_2 heterostructure; a) in a separate state; b) in an equilibrium state of contact; and c) the PANi/TiO_2 heterostructure is excited by light.

reactive oxygen species can react with the PANi by means of the outer sphere electron transfer that behaves as acceptor-like dopants in the *p*-type PANi semiconductor. On the other hand, the reactive oxygen species can eliminate some donor-like dopants such as reductive agents physically adsorbed on the PANi surface. An increase in acceptor-like dopants in accompaniment with a de-doping of donor-like dopants at the irradiation start leads to an abrupt increase in hole density that accounts for the sudden drop in resistance of the PANi component layer. As the electrochemical process is going on, the oxidation degree of the PANi component layer is expected to

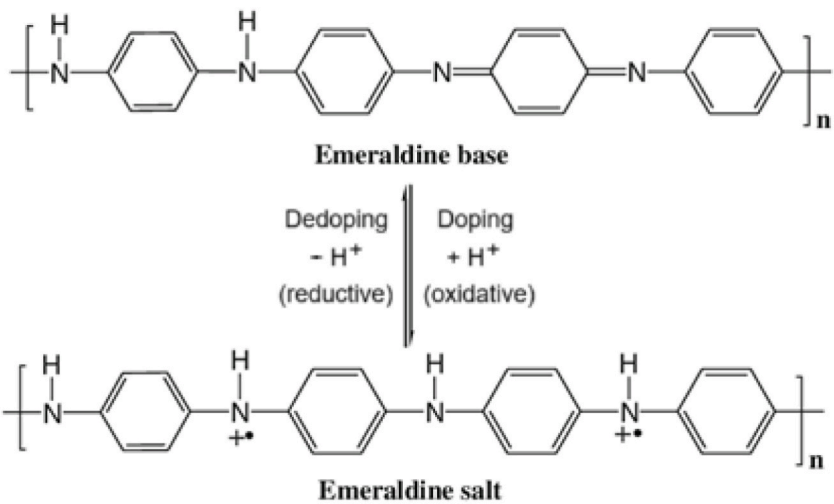

Fig. 10. The inversion between PANi emeraldine base and emeraldine salt due to the oxidation and reduction process.

increase; the initial PANi emeraldine salt gradually inverts to the PANi emeraldine base, resulting in a reduction in its conductance. As a result, a slowdown in the light sensitivity and a U-turn in the resistance baseline are observed. The light response of the PANi component reveals the fact that the electrochemical effect is dominated at the start of light irradiation but gradually declines, resulting in a conversion from the positive to negative mode. The conversion point CP is assumed to be the balance between the photoelectronic and electrochemical effects. The response observed with the excitation light of wavelength 447 nm indicates the presence of reactive oxygen species, indicating a fact that the photoinduction in the PANi/TiO_2 heterostructure is expanded to the blue light region. With the excitation light of wavelength 663 nm, no electrons are photogenerated in the TiO_2 component, but the holes in the PANi component, no reactive radicals appear, and the light response of the PANi component layer is simply identical to that of the pristine PANi layer.

4. Conclusions

The experiment has shown a correlation between the conductance of the PANi component and the photoinduction features of the PANi/TiO_2 heterogeneous structure in open air. In terms of light sensitivity, the response of the PANi component is accounted for by the modifications of both the photoelectronic and the electrochemical processes that associate with the photoinduction taking place inside and outside over the PANi/TiO_2 heterojunction. The photoelectronic modification involves the excess electrons and holes photogenerated in the TiO_2 and PANi sides that can modify the depletion region of the heterostructure. As a consequence of the following thermal diffusion of the excess charges across the heterojunction, the width of the depletion are altered, leading to a change in the conductance of the structure components, including PANi. On the other hand, the electrochemical modification relates to the effect of the reactive oxygen species of $O_2^{\bullet -}$, $OH^{\bullet -}$ and H^+ that are created over the PANi/TiO_2 heterojunction. Acting as secondary acceptor-like dopants and donor-like de-dopants, the reactive radicals boost the extraction of electrons from PANi chain and fast raise the hole density of the *p*-type semiconductor PANi at the irradiation start. However, as the irradiation is going on, the excess reactive oxygen species alter the oxidation degree of the PANi then gradually invert the initial PANi emeraldine salt to the emeraldine base, resulting in a reduction of the PANi layer conductance. The combination of two modifications is explained for the mixing response of the PANi conductance and the U-turn shape of its baseline. The appearance of reactive oxygen species over the PANi/TiO_2 upon exposure to the excitation light in open air could be used as an effective means to sterilise bacteria or clean up some airborne pollutants.

CRediT authorship contribution statement

Huyen Ngoc Duong: Writing – review & editing, Writing – original draft, Supervision, Funding acquisition, Conceptualization. **Tan Van Le:** Writing – review & editing, Writing – original draft, Supervision, Formal analysis, Data curation.

Data and code availability

The pictures, Raman, UV–Vis and sensitivity graphs in Origin file which containing both graph and measuring data are provided upon request.

Ethical approval

Not applicable, the experiments do not involve to human tissue.

Declaration of competing interest

The authors declare the following financial interests/personal relationships which may be considered as potential competing interests: Duong Ngoc Huyen reports a relationship with Industrial University of Ho Chi Minh City that include employment. If there are other authors, they declare that they have no known competing financial interests or personal relationships that could have appeared to influence the work reported in this paper.

Acknowledgements

The work is carried on thanks to the fund from Industrial University of Ho Chi Minh City (IUH) via the Research Contract No. 241/HDLD.

Supplementary information:

Not applicable.

References

[1] A. Fujishima, K. Honda, Electrochemical photolysis of water at a semiconductor electrode, Nature 238 (1972) 37–38, https://doi.org/10.1038/238037a0.
[2] K. Hashimoto, H. Irie, A. Fujishima, TiO_2 photocatalysis: a historical overview and future prospects, Jpn. J. Appl. Phys. 44 (2005) 8269, https://doi.org/10.1143/JJAP.44.8269.
[3] T. Matsunaga, R. Tomoda, T. Nakajima, H. Wake, Photoelectrochemical sterilization of microbial cells by semiconductor powders, FEMS Microbiol. Lett. 29 (1985) 211, https://doi.org/10.1111/j.1574-6968.1985.tb00864.x.
[4] C. Trapalis, P. Keivanidis, G. Kordas, M. Zaharescu, M. Crisan, A. Szatvanyi, M. Gartner, $TiO_2(Fe^{3+})$ nanostructured thin films with antibacterial properties, Thin Solid Films 433 (2003) 186, https://doi.org/10.1016/S0040-6090(03)00331-6.
[5] J. Wang, J. Polleux, J. Lim, B. Dunn, Pseudocapacitive contributions to electrochemical energy storage in TiO_2 (anatase) nanoparticles, J. Phys. Chem. C 111 (2007) 14925, https://doi.org/10.1021/jp074464w.
[6] M.S.S. Danish, A. Bhattacharya, D. Stepanova, A. Mikhaylov, M.L. Grilli, M. Khosravy, T. Senjyu, A systematic review of metal oxide applications for energy and environmental sustainability, Metals 10 (12) (2020) 1604, https://doi.org/10.3390/met10121604.
[7] R. Medhi, M.D. Marquez, T.R. Lee, Visible-light-Active doped metal oxide nanoparticles: review of their synthesis, properties, and applications, ACS Appl. Nano Mater. 3 (2020) 6156, https://doi.org/10.1021/acsanm.0c01035.
[8] S. Ghosh, N. Kouamé, L. Ramos, et al., Conducting polymer nanostructures for photocatalysis under visible light, Nat. Mater. 14 (2015) 505, https://doi.org/10.1038/nmat4220.
[9] H. Dong, G. Zeng, L. Tang, C. Fan, C. Zhang, X. He, Y. He, An overview on limitations of TiO_2-based particles for photocatalytic degradation of organic pollutants and the corresponding countermeasures, Water Res. 79 (2015) 128, https://doi.org/10.1016/j.watres.2015.04.038.
[10] R. Ghamarpoor, A. Fallah, M. Jamshidi, A review of synthesis methods, modifications, and mechanisms of ZnO/TiO2-based photocatalysts for photodegradation of contaminants, ACS Omega 9 (24) (2024) 25457, https://doi.org/10.1021/acsomega.3c08717.
[11] H. Park, Y. Park, W. Kim, W. Choi, Surface modification of TiO_2 photocatalyst for environmental applications, J. Photochem. Photobiol. C Photochem. Rev. 15 (2013) 1–20, https://doi.org/10.1016/j.jphotochemrev.2012.10.001.
[12] T.J. Pawar, D. Contreras López, J.L. Olivares Romero, J.V. Montesinos, Surface modification of titanium dioxide, J. Mater. Sci. 58 (2023) 6887, https://doi.org/10.1007/s10853-023-08439-x.
[13] F.R. Fan, A.J. Bard, Spectral sensitization of the heterogeneous photocatalytic oxidation of hydroquinone in aqueous solution at phthalocyanine-coated TiO_2 powders, J. Am. Chem. Soc. 101 (1979) 6139, https://doi.org/10.1021/ja00514a056.
[14] J.M. Herrmann, Heterogeneous photocatalysis: fundamentals and applications to the removal of various types of aqueous pollutants, Catal. Today 53 (1999) 115, https://doi.org/10.1016/S0920-5861(99)00107-8.
[15] R. Marschall, Semiconductor composites: strategies for enhancing charge carrier separation to improve photocatalytic activity, Adv. Funct. Mater. 24 (2014) 2421–2440, https://doi.org/10.1002/adfm.201303214.
[16] H. Wang, L. Zhang, Z. Chen, et al., Semiconductor heterojunction photocatalysts: design, construction, and photocatalytic performances, Chem. Soc. Rev. 43 (2014) 5234–5244, https://doi.org/10.1039/C4CS00126E.
[17] H. Wang, X. Li, X. Zhao, C. Li, X. Song, P. Zhang, P. Huo, X. Xin, A review on heterogeneous photocatalysis for environmental remediation: from semiconductors to modification strategies, Chin. J. Catal. 43 (2) (2022) 178, https://doi.org/10.1016/S1872-2067(21)63910-4.
[18] A.G. MacDiarmid, R.J. Mammone, R.B. Kaner, S.J. Porter, The concept of 'doping' of conducting polymers. The role of reduction potentials, Phil. Trans. Roy. Soc. Lond. 314 (1985) 3. https://www.researchgate.net/publication/261143308.
[19] J.R. Reynolds, B.C. Thompson, T.A. Skotheim (Eds.), Conjugated Polymers Perspective, Theory, and New Materials, fourth ed., CSR Press, 2019 https://doi.org/10.1201/b22235.
[20] G. Saianand, A.I. Gopalan, L. Wang, K. Venkatramanan, V.A. Roy, P. Sonar, D. Lee, R. Naidu, Conducting polymer based visible light photocatalytic composites for pollutant removal: progress and prospects, Environ. Technol. Innovat. 28 (2022) 10698, https://doi.org/10.1016/j.eti.2022.102698.
[21] A.F. Diaz, J.A. Logan, Electroactive polyaniline films, J. Electroanal. Chem. 111 (1) (1980) 111, https://doi.org/10.1016/S0022-0728(80)80081-7.
[22] A.G. MacDiarmid, A.J. Epstein, Polyanilines - a novel class of conducting polymers, Faraday Discuss J Chem Soc 88 (1989) 317, https://doi.org/10.1039/DC9898800317.
[23] W.S. Huang, A.G. MacDiarmid, Optical properties of polyaniline, Polymer 34 (1993) 1833, https://doi.org/10.1016/0032-3861(93)90424-9.
[24] J. Libert, J. Cornil, D.A. Dos Santos, J.L. Bredas, From neutral oligoanilines to polyanilines: a theoretical investigation of the chain-length dependence of the electronic and optical properties, Phys. Rev. B 56 (1997) 8638, https://doi.org/10.1103/PhysRevB.56.8638.
[25] J. Stejskal, M. Trchová, P. Bober, P. Humpolíček, V. Kašpárková, I. Sapurina, M.A. Shishov, M. Varga, Conducting polymers: polyaniline, in: Encyclopedia of Polymer Science and Technology, 2002, pp. 1–44, https://doi.org/10.1002/0471440264.pst640.
[26] K. Namsheer, C.S. Rout, Conducting polymers: a comprehensive review on recent advances in synthesis, properties and applications, RSC Adv. 11 (10) (2021) 5659–5697, 10.1039%2Fd0ra07800j.
[27] Z. Liu, J. Zhou, H. Xue, L. Shen, H. Zang, W. Chen, Polyaniline/TiO_2 solar cells, Synth. Met. 156 (2006) 721–723, https://doi.org/10.1016/j.synthmet.2006.04.001.
[28] D.N. Huyen, N.T. Tung, N.D. Thien, L.H. Thanh, Effect of TiO_2 on the gas sensing features of TiO_2/PANi nanocomposites, Sensors 11 (2011) 1924–1931, 10.3390%2Fs110201924.
[29] O.S. Ekande, M. Kumar, Review on polyaniline as reductive photocatalyst for the construction of the visible light active heterojunction for the generation of reactive oxygen species, J. Environ. Chem. Eng. 9 (4) (2021) 105725, https://doi.org/10.1016/j.jece.2021.105725.
[30] K.R. Reddy, K.V. Karthik, S.B. Benaka Prasad, K.S. Sarvesh, M.J. Han, V.R. Anjanapura, Enhanced photocatalytic activity of nanostructured titanium dioxide/polyaniline hybrid photocatalysts, Polyhedron 120 (2016) 169–174, 10.1016%2Fj.poly.2016.08.029.
[31] N.K. Jangid, S. Jadoun, A. Yadav, M. Srivastava, N. Kaur, Polyaniline/TiO_2 based photocatalysts for dyes degradation, Polym. Bull. 78 (12) (2021) 4743. https://link.springer.com/article/10.1007/s00289-020-03318-w.
[32] X. Deng, Y. Chen, J. Wen, Y. Xu, J. Zhu, Z. Bian, Polyaniline-TiO_2 composite photocatalysts for light-driven hexavalent chromium ions reduction, Sci Bull (Beijing) 65 (2020) 105–112, https://doi.org/10.1016/j.scib.2019.10.020.
[33] Y. Fu, M. Janczarek, Polyaniline–titanium dioxide heterostructures as efficient photocatalysts: a review, Crystals 13 (2023) 1637, https://doi.org/10.3390/cryst13121637.
[34] D.N. Huyen, M.V. Tuan, M.X. Dung, Charge photogeneration and transfer in polyaniline/titanium dioxide heterostructure, Catalysts 14 (9) (2024) 585, https://doi.org/10.3390/catal14090585.
[35] S.K. Singh, X. Crispin, I. Zozoulenko, Oxygen reduction reaction in conducting polymer PEDOT: density functional theory study, J. Phys. Chem. C 121 (22) (2017) 12270–12277, https://doi.org/10.1021/acs.jpcc.7b03210.
[36] V. Gueskine, A. Singh, M. Vagin, X. Crispin, I. Zozoulenko, Molecular oxygen activation at a conducting polymer: electrochemical oxygen reduction reaction at PEDOT revisited, a theoretical study, J. Phys. Chem. C 124 (24) (2020) 13263–13272, https://doi.org/10.1021/acs.jpcc.0c03508.
[37] I. Sapurina, A. Riede, J. Stejskal, In-situ polymerized polyaniline films: 3. Film formation, Synth. Met. 105 (1999) 195, https://doi.org/10.1016/S0379-6779(01)00349-6.
[38] D.N. Huyen, T.V. Ky, L.H. Thanh, In situ chemically polymerized polyaniline nanolayer: characterizations and sensing materials, J. Exp. Nanosci. 4 (3) (2009) 203–212, https://doi.org/10.1080/17458080903236407.
[39] N.T. Tung, D.N. Huyen, Effect of HCl on the formation of TiO_2 nanocrystallites, J. Nanomater. ID 6547271 (2016), https://doi.org/10.1155/2016/6547271.
[40] D.N. Huyen, Mechanical characterization of polyaniline film chemically growth on glass substrate, Asian J. Phys. 30 (12) (2021) 1667.
[41] U.P. Balachandran, N.G. Eror, Raman spectra of titanium dioxide, J. Solid State Chem. 42 (1982) 276, https://doi.org/10.1016/0022-4596%2882%2990006-8.

[42] M. Trchová, Z. Morávková, M. Bláha, J. Stejskal, Raman spectroscopy of polyaniline and oligoaniline thin films, Electrochim. Acta 122 (2014) 28–38, https://doi.org/10.1016/j.electacta.2013.10.133.
[43] M.I. Boyer, S. Quillard, E. Rebourt, G. Louarn, J.P. Buisson, A. Monkman, S. Lefrant, Vibrational analysis of polyaniline: a model compound approach, Phys. Chem. B 102 (1998) 7382, https://doi.org/10.1021/jp972652o.
[44] S. Quillard, G. Louarn, S. Lefrant, A.G. MacDiarmid, Vibration analysis of polyaniline: a comparative study of leucoemeradine, emeradine and pernigraniline, Phys. Rev. B 50 (1994) 12496, https://doi.org/10.1103/PhysRevB.50.12496.
[45] J.E.P. Da Silva, Torresi SIC. De, D.L.A. De Faria, M.L.A. Temperini, Raman characterization of polyaniline induced conformational changes, Synth. Met. 101 (1999) 834.
[46] S. Stafström, J.L. Brédas, A.J. Epstein, H.S. Woo, D.B. Tanner, W.S. Huang, A.G. MacDiarmid, Polaron lattice in highly conducting polyaniline: theoretical and optical studies, Phys. Rev. Lett. 59 (1987) 1464, https://doi.org/10.1103/PhysRevLett.59.1464.
[47] M.N. Gustavo, A.S. Marcelo, Spectroscopy of nanostructured conducting polymers, in: Ali Eftekhari Ed Nanostructured Conductive Polymers, Wiley & Sons, 2010, pp. 341–373. https://onlinelibrary.wiley.com/doi/10.1002/9780470661338.ch8.